10.1098/rspa.2002.0959

THE ROYAL SOCIETY

Coronal heating by the phase mixing of individual pulses propagating in coronal holes

By A. W. Hood, S. J. Brooks and A. N. Wright
School of Mathematics and Statistics, St Andrews University, St Andrews KY16 9SS, UK

Received 18 May 2001; revised 17 December 2001; accepted 2 January 2002
published online 16 August 2002

The propagation of Alfvénic pulses into an inhomogeneous model of a coronal hole is investigated. It is demonstrated that the standard exponential damping of a harmonically generated wavetrain, due to phase mixing, is replaced by a slower algebraic damping when individual pulses are considered, suggesting that pulses will transport energy higher into the corona than a wavetrain. In addition, the initial shape of the pulse is rapidly transformed into a travelling Gaussian pulse. When two pulses of opposite sign travelling in the same direction are generated, the pulses diffuse into each other and the decay of the amplitude is faster, although still algebraic.

Keywords: Sun; magnetic fields; coronal heating; wave propagation

1. Introduction

Phase mixing of Alfvén waves has been suggested as a possible heating mechanism for the open-field regions of coronal holes in the solar corona. It is difficult for open magnetic field lines to become stressed and to store magnetic energy *in situ*. Thus the magnetic field in coronal holes is nearly potential, with no free energy available for heating. Any photospheric motions move the magnetic footpoints, but these motions do not store energy in the coronal magnetic field, instead they excite magnetohydrodynamic (MHD) waves that propagate into the coronal hole. However, the horizontal Alfvén speed within a coronal hole need not be uniform and clear evidence of non-uniformity in the plasma density is seen in coronal plumes (DeForest *et al*. 1997, 2001), with the plume having up to five times the density of the inter-plume plasma. On the edge of the plume, the density rises rapidly. Since the low-β coronal plasma is dominated by the magnetic field, meaning that there are no rapid changes in the field, there will be strong horizontal gradients in the coronal Alfvén speed, $V_{\mathrm{A}}(x)$. Thus any disturbances that are generated by either photospheric footpoint motions or magnetic reconnection of colliding photospheric flux elements must propagate into a plasma that has a non-uniform Alfvén speed.

Phase mixing remains a possible mechanism for damping any disturbances excited on open-field lines. The mechanism can be thought of along the following lines. Since plasma inhomogeneities result in a spatially varying Alfvén speed in the corona, it is possible that disturbances at the photospheric base of the coronal hole will propagate along different magnetic field lines at different speeds. Waves will quickly become out of phase with each other and extremely large horizontal gradients will develop. The gradients continue to build up until the effect of dissipation, through either resistivity or viscosity, limits the growth and the waves become damped. The damping can be quite dramatic, with a damping length depending on the dissipation coefficient to the power of one third. If the vertical direction is z, the horizontal direction of inhomogeneity is x and the ignorable direction is y, then typically when the boundary at $z = 0$ is excited harmonically as $\cos(\omega t)$ the Alfvén wave behaves like

$$\cos[(k(x)z - \omega t)] \exp(-\epsilon z^3),$$

where $k(x) = \omega / V_{\mathrm{A}}(x)$ and $\epsilon = \eta\omega^2 (V_{\mathrm{A}}')^2 / 6V_{\mathrm{A}}^5$ is proportional to the resistivity, η, and to the square of the derivative of the Alfvén speed, $V_{\mathrm{A}}'(x)$. With the lower boundary being driven harmonically, this means that the phase mixing occurs in space.

Phase mixing can also occur in time (see Heyvaerts & Priest 1983; Mann *et al*. 1997; Hood *et al*. 1997). In this case, the initial disturbance is sinusoidal in z and standing waves dissipate rapidly in time due to phase mixing. Thus, for the initial condition of the form $\cos(kz)$, the wave decays as

$$\exp[\mathrm{i}(kz - \omega(x)t)] \exp(-\epsilon t^3),$$

where $\omega(x) = kV_{\mathrm{A}}(x)$ and, in this case, $\epsilon = \frac{1}{6}\eta k^2 (V_{\mathrm{A}}')^2$. Again, ϵ is proportional to η and $(V_{\mathrm{A}}')^2$. Cally (1991) interprets this development of short time-scales as a cascade of energy to higher Fourier modes, in a manner similar to turbulence.

However, the basic investigations by Heyvaerts & Priest (1983) and the subsequent developments by Parker (1991), Hood *et al*. (1997), Ruderman *et al*. (1998) and De Moortel *et al*. (1999, 2000) have all assumed that the waves are generated by exciting an infinite wavetrain of sinusoidal oscillations due to photospheric motions. Other authors have investigated nonlinear effects. Botha *et al*. (2000) showed that the nonlinear coupling of Alfvén waves to fast waves is actually quite inefficient. The fast wave amplitude saturates at a level related to the square of the Alfvén wave amplitude.

In reality, it is extremely unlikely that an infinite wavetrain will be generated and instead it is more likely that only one or at most a few pulses will be excited by boundary motions. So the basic questions investigated in this paper are the following. How does a single-pulse phase mix in an inhomogeneous plasma? Are there any differences to the standard phase mixing results of Heyvaerts & Priest (1983)? Sakurai & Granik (1984) did investigate the effect of a random photospheric footpoint driver, but restricted attention to closed field lines in coronal loops. They considered both surface waves and small variations in the Alfvén speed profile, including coupling between Alfvén and fast magnetoacoustic waves.

The propagation of a single pulse is investigated in § 3 by numerically solving the linearized MHD equations. A simple model of a coronal hole structure is used, but the basic physics is retained. The evolution is investigated by studying how the amplitude decays and how the width of the pulse changes in time. Next, two pulses of opposite sign are generated and the evolution followed in § 4. Section 5 presents an analytic description of an individual pulse and the two pulses. The final section discusses the implications for wave propagation in coronal holes, the deposition of the pulse energy and the implications for heating coronal plumes.

2. The basic equations

The equilibrium is taken as a uniform vertical magnetic field with a structured density profile in the horizontal direction. This simple model of a coronal hole illustrates the basic properties of wave propagation in a structured plasma. Hence

$$\boldsymbol{B}_0 = B_0 \boldsymbol{e}_z, \qquad \rho = \rho(x). \tag{2.1}$$

Therefore, the Alfvén speed, $V_\mathrm{A}(x)$, defined by $V_\mathrm{A}^2 = B_0^2/\mu\rho$, varies from field line to field line. Previous work has shown that a simple harmonic wave will propagate with different speeds on different field lines. The waves quickly become out of phase with each other and large horizontal gradients build up. In this manner, short length-scales are created and dissipation eventually damps the waves. This phase-mixing mechanism (Heyvaerts & Priest 1983) has been investigated in various situations by De Moortel *et al*. (1999, 2000), Ruderman *et al*. (1998), Botha *et al*. (2000) and Steinolfson (1985). All of these authors have concentrated on an infinite harmonic wavetrain. In this paper we focus on the behaviour of an individual pulse and investigate the differences with an infinite wavetrain. So an initial disturbance is given near $z = 0$ with an initial velocity that ensures it propagates up into the coronal hole and, in the next section, the resulting disturbance is followed numerically.

The linearized Alfvén wave equation in an inhomogeneous plasma is

$$\frac{\partial^2 b_y}{\partial t^2} = V_\mathrm{A}^2(x)\frac{\partial^2 b_y}{\partial z^2} + \eta\frac{\partial}{\partial t}\frac{\partial^2 b_y}{\partial x^2}, \tag{2.2}$$

where b_y is the perturbed magnetic field component corresponding to an Alfvénic disturbance. Note that we only keep the x derivatives in the diffusion term and drop the additional term

$$\frac{\partial}{\partial t}\frac{\partial^2 b_y}{\partial z^2}.$$

It always remains small compared with the first term on the right-hand side. This assumption is not essential for the numerical results, but neglecting the extra diffusion term is needed for analytical progress.

A more realistic coronal-hole model would assume cylindrical geometry, where b_y is replaced by b_θ and $V_\mathrm{A}(x)$ by $V_\mathrm{A}(R)$, and the diffusion term becomes

$$\eta\frac{\partial}{\partial t}\left(\frac{1}{R}\frac{\partial}{\partial R}\left(R\frac{\partial b_\theta}{\partial R}\right)\right).$$

If the variation in the Alfvén speed occurs near the radius d and over a length-scale l, then (2.2) is a realistic approximation, provided $l \ll d$.

The initial conditions at $t = 0$ are taken as

$$b_y = F(z), \tag{2.3}$$

$$\frac{\partial b_y}{\partial t} = -V_\mathrm{A}(x)F'(z). \tag{2.4}$$

This ensures that the pulse propagates into the computational domain and that the lower boundary effects are unimportant.

If an infinite number of waves had been selected, then the initial condition would have been

$$b_y = \cos kz$$

and the ideal undamped Alfvén wave would have had the form

$$b_y = \cos(kz - \omega t).$$

The dispersion relation then relates the frequency, ω, and the wavenumber, k,

$$\omega = kV_{\mathrm{A}}(x).$$

The analysis of Heyvaerts & Priest (1983) shows that the Alfvén wave phase mixes in time as

$$b_y = \exp(\mathrm{i}kz - \mathrm{i}\omega t)\exp(-\tfrac{1}{6}\eta k^2 (V_{\mathrm{A}}')^2 t^3).$$

Thus the wavetrain is damped *exponentially* with a power of t^3 and the damping time depends on $\eta^{-1/3}$.

3. Individual pulse propagation

Here, results obtained from time-stepped two-dimensional numerical simulations of (2.2) are presented. The numerical method used was a centred sixth-order finite-difference scheme with a third-order Runge–Kutta-based time-step. This method is well suited to linear wave propagation in the absence of shocks. To solve equation (2.2) numerically, it is expressed in the dimensionless form

$$\frac{\partial U}{\partial t} = V_{\mathrm{A}}^2(x)\frac{\partial^2 b_y}{\partial z^2} + \eta\frac{\partial^2 U}{\partial x^2}, \tag{3.1}$$

$$\frac{\partial b_y}{\partial t} = U, \tag{3.2}$$

where $x = \bar{x}L$, $z = \bar{z}L$, $V_{\mathrm{A}} = V_{\mathrm{A0}}\bar{V}_{\mathrm{A}}$, $t = \bar{t}L/V_{\mathrm{A0}}$, $\bar{\eta} = \eta/LV_{\mathrm{A0}}$ and $\rho = \bar{\rho}\rho_0$. L is the half-width of the inhomogeneous plasma structure and $V_{\mathrm{A0}} = B_0/\sqrt{\mu\rho_0}$ is the typical Alfvén speed. Bars are now dropped for convenience.

$$V_{\mathrm{A}}(x) = \tfrac{1}{2}\cos(\pi x) + 1 \tag{3.3}$$

is chosen as the functional form of the dimensionless Alfvén speed.

The magnetic-field component $b_y(x, z, t)$ is solved on the discretized spatial domain

$$D = [x_i, z_j], \quad x, z \in \{0, 1, 2, \dots, N_x; 0, 1, 2, \dots, N_z\}, \tag{3.4}$$

with $x(N_x) = 1$ and $z(N_z) = z_{\max}$, with $z_{\max}$ selected by how far the initial pulse is followed.

The first case considered involves a single pulse propagating away from the bottom boundary ($z = 0$). The second case considers an additional section of the pulse having the opposite sign to the first part. The boundary conditions are taken as

$$\frac{\partial b_y}{\partial x} = 0 \quad \text{for } x = 0 \text{ and } x = 1, \tag{3.5}$$

$$b_y(x, 0, t) = 0. \tag{3.6}$$

There is no condition set on the boundary $z = z_{\max}$, as the simulation terminates before the arrival of any pulse. Note that there is no variation in x in the initial profile and that variations in x are generated entirely by the propagation of the pulse in an inhomogeneous plasma. Nocera *et al.* (1984) investigate how an infinite wavetrain, that is initially localized about a particular field line, spreads out and becomes defocused as a result of phase mixing.

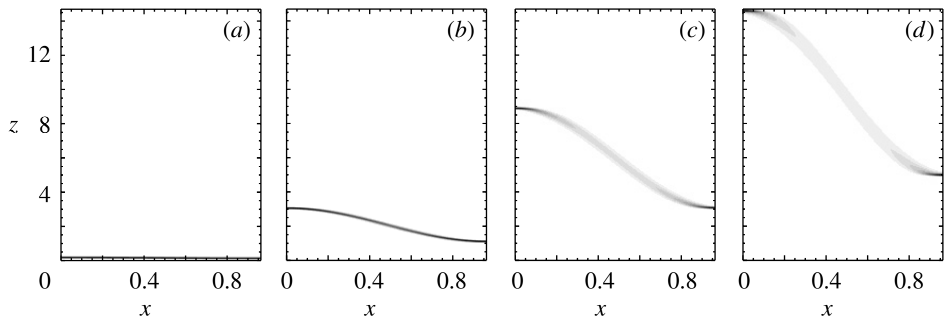

Figure 1. Snapshots of b_y at given times, showing the non-uniform propagation and dissipation of the pulse, $\eta = 5 \times 10^{-4}$. (*a*) $t = 0$; (*b*) $t = 2.0$; (*c*) $t = 6.0$; (*d*) $t = 9.9$. Note the different scales on the x- and z-axes.

(*a*) *Single pulse*

The initial conditions for b_y and U, creating a single pulse, are

$$b_y(x,z,t=0) = \begin{cases} 1+\cos(10\pi(z-\frac{1}{10})), & 0 < z < \frac{2}{10}, \\ 0, & \text{elsewhere}, \end{cases} \tag{3.7}$$

$$U(x,z,t=0) = \begin{cases} n\pi V_{\mathrm{A}}(x)\sin(10\pi(z-\frac{1}{10})), & 0 < z < \frac{2}{10}, \\ 0, & \text{elsewhere}, \end{cases} \tag{3.8}$$

where these equations express the relation between b_y and U for an Alfvén wave, namely

$$U = \frac{\partial b_y}{\partial t} = -V_{\mathrm{A}}(x)\frac{\partial b_y}{\partial z},$$

that is propagating vertically up in an ideal plasma.

(*b*) *Structural development*

The pulse is initially invariant in the x-direction and propagates in the increasing z-direction (upwards), as can be seen in the time-dependent snapshots shown in figure 1. In the region of D where $x < 0.5$ that section of the pulse travels faster than its counterpart in $x > 0.5$, due to the choice of the Alfvén speed profile in (3.3). The darker shades represent the stronger magnetic field and vice versa. The magnetic field is seen clearly to diffuse as the stronger gradients in the x-direction develop due to the horizontal variation in the Alfvén speed. (Note the different scales for the x- and z-axes.) Cross-section cuts along $x = 0.5$ show that the pulse profile quickly transforms into a Gaussian shape of the form

$$b_y = A\mathrm{e}^{-(z-z_1)^2/2d^2}, \tag{3.9}$$

where A is the amplitude, z_1 is the height of the maximum of b_y and d is the width. The amplitude, A, decays as the pulse propagates up into the coronal hole, due to damping through phase mixing, and the width increases with time. These variations are investigated below. A similar Gaussian behaviour is found in the horizontal direction. This is illustrated by selecting the height z_1 that corresponds to the maximum of b_y at $x = 0.5$. Then a cut is taken in the horizontal direction at $z = z_1$.

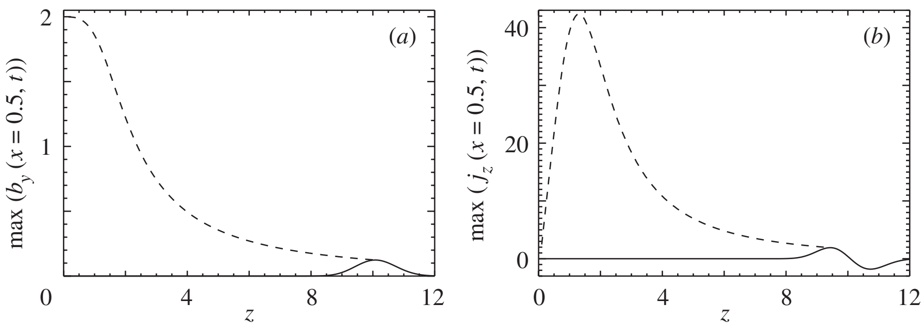

Figure 2. The dashed line is the tracked maximum value of $b_y(x = 0.5, z)$ and $j_z(x = 0.5, z)$. The solid line is the profile of $b_y(x = 0.5, z)$ and $j_z(x = 0.5, z)$ at $t = 10$ for $\eta = 5 \times 10^{-4}$.

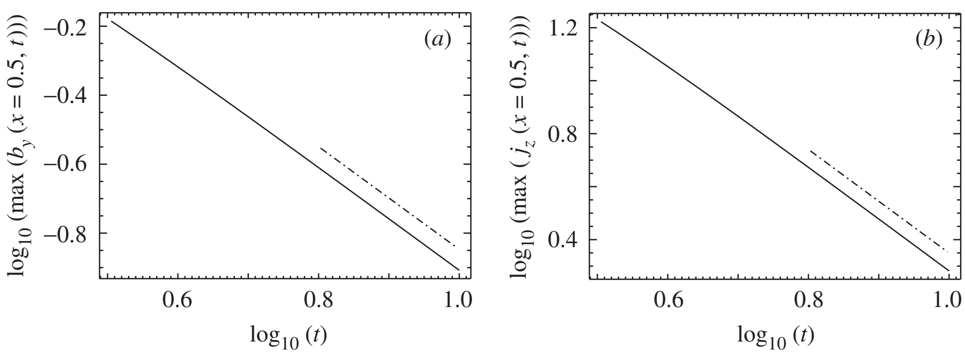

Figure 3. The decay rate of (a) max(b_y) and (b) j_z at $x = 0.5$. The dot-dashed line is the (displaced) least-squares fit with (a) gradient = −1.49 and (b) gradient = −1.97.

(c) *Amplitude decay rate*

The decay of the amplitudes of b_y and the current j_z can be monitored during the simulation. The dashed lines in figure 2 show how the maximum values of $b_y(x = 0.5, z, t)$ and $j_z(0.5, z, t)$ vary with z. The solid line shows the final profile of $b_y(x = 0.5, z, 10)$ at time $t = 10$ and the similarity with a Gaussian profile is clearly evident. At very early times, before there is any significant development in the gradients across x, the decay is minimal but then the amplitude decreases rapidly before the rate of decrease slows at later times. For large t, the decay is shown in figure 3 to follow power laws in t of the form

$$\max(b_y(0.5, z, t)) = A = k_1 t^{-3/2} \quad \text{and} \quad \max(j_z(0.5, z, t)) = J = k_2 t^{-2}. \tag{3.10}$$

The dashed line is the least-squares fit to the decay, with a gradient of −1.49, which, in the limit of large t, tends to $-\frac{3}{2}$. The straightness of the solid line clearly demonstrates the close fit to the power law in t. The dashed line has been artificially displaced to show that the lines are parallel, but in fact it actually lies directly on top of the solid line. Numerical results show this decay rate exponent for an individual pulse does not display any dependence on the initial conditions, the value of η or on $V_{\mathrm{A}}(x)$. This power-law decay is completely different from the exponential damping found for an infinite wavetrain (see Heyvaerts & Priest 1983). The constant k_1, however, does depend on η and $V_{\mathrm{A}}(x)$ and this is investigated later. Note that, at $x = 0.5$, $V_{\mathrm{A}}(0.5) = 1$ and $V_{\mathrm{A}}'(0.5) = \frac{1}{2}\pi$ for the chosen profile.

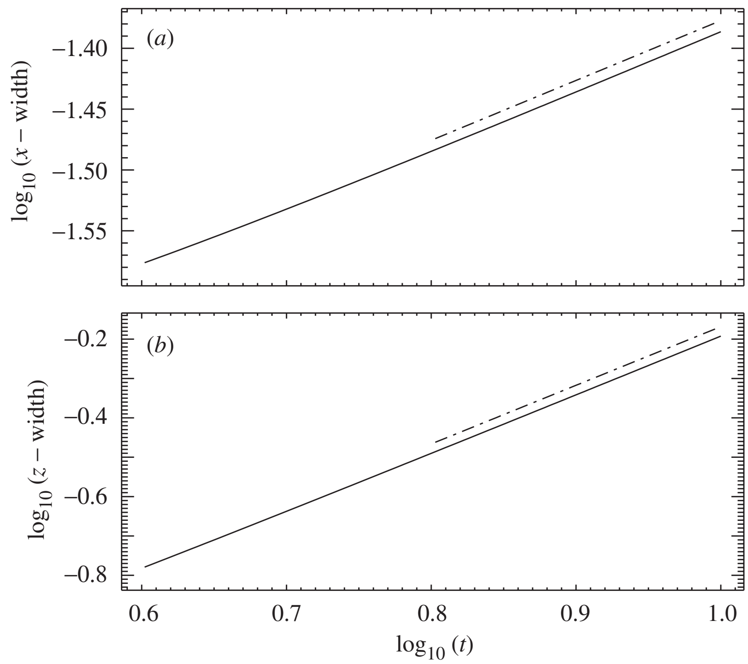

Figure 4. The growth in the width of the pulse in both the x- (gradient = 0.49) and the z- (gradient = 1.49) directions. The dot-dashed line is the (displaced) least-squares fit and $\eta = 5 \times 10^{-4}$.

(*d*) *Width of the pulse*

Another feature of the propagating pulse is the increase in its width accompanying the decrease in amplitude. The rate of increase in the width of the pulse can be measured numerically and the width d analysed as a time-series. The data in either the x-direction with z fixed or the z-direction with $x = 0.5$ are fitted by a single Gaussian. The standard deviation of the fitted Gaussian is used as a measure of the width. The width in the z-direction is measured for successive time-intervals at $x = 0.5$. The width in the x-direction is taken, similarly, at the index in z where the maximum value of b_y at $x = 0.5$ lies. Figure 4 shows this typical behaviour for the single pulse experiment with the dimensionless resistivity, $\eta = 5 \times 10^{-4}$.

The width of the Gaussian pulse in the x-direction is given by $d_x = k_x t^{1/2}$ and for the z-direction $d_z = k_z t^{3/2}$. The rate of increase in the width, as for the amplitude, does not display any dependence on either the initial conditions, the value of η or the form of $V_A(x)$. k_x and k_z do depend on η and $V_A(x)$ and they are calculated for different values of η below. The reason for the different power laws in d_x and d_z is explained in § 5.

(*e*) *Variation of* η

The effect of the variation of η on the system is studied through a series of six simulations, each with a different value of η. Changing η in (3.1) produces a change in value of k_1 in (3.10) and also produces corresponding changes in the two width parameters k_x and k_z.

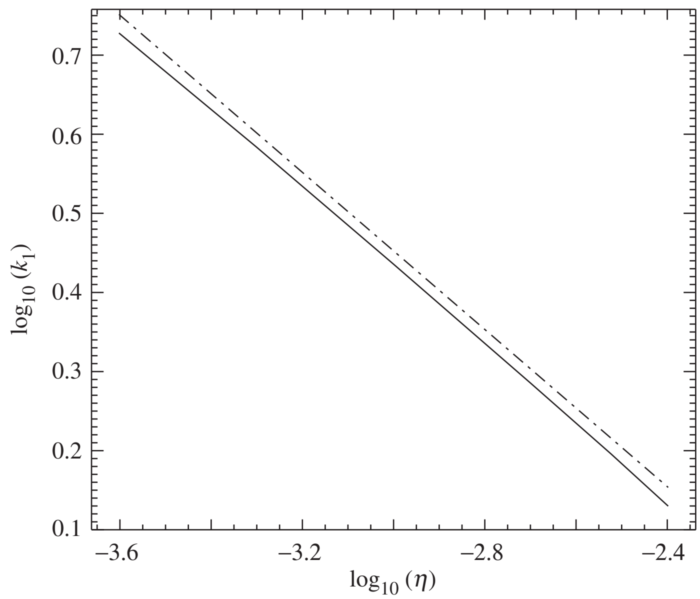

Figure 5. Relationship between k_1 and η (gradient $= -0.5$). The dot-dashed line is the (displaced) least-squares fit.

The relationship between k_1 and η is shown clearly in figure 5 to be a power law of the form

$$k_1 = c_1 \eta^{-1/2}. \tag{3.11}$$

Hence, from (3.10) and (3.11), the damping time for the amplitude is proportional to $\eta^{-1/3}$. However, although this scaling is the same as the Heyvaerts & Priest (1983) result, the decay is now only algebraic, rather than exponential in time.

The value of the constant c_1 is calculated from the least-squares fit to be $10^{-1.06}$. In a similar fashion, we find power laws for the relationship between k_x and k_z and the corresponding constants c_x and c_y are calculated from the least-squares fit to be $10^{-0.28}$ and $10^{-0.16}$, respectively, as shown in figure 6. Summarizing, the numerical simulations give

$$A = 0.087 \eta^{-1/2} t^{-3/2}, \tag{3.12}$$

$$J = 0.094 \eta^{-1} t^{-2}, \tag{3.13}$$

$$d_x = 0.525 \eta^{1/2} t^{1/2}, \tag{3.14}$$

$$d_z = 0.692 \eta^{1/2} t^{3/2}. \tag{3.15}$$

4. Bipolar pulse

The simulation from the above section is extended to the case where a bipolar pulse propagates into the coronal hole. The same shape of pulse is considered, but the second pulse has the opposite sign. Thus we take

$$b_y(x, z, t = 0) = \begin{cases} 1 + \cos(10\pi(z - \frac{3}{10})), & \frac{2}{10} < z < \frac{4}{10}, \\ -1 - \cos(10\pi(z - \frac{1}{10})), & 0 < z < \frac{2}{10}, \\ 0, & \text{elsewhere}, \end{cases} \tag{4.1}$$

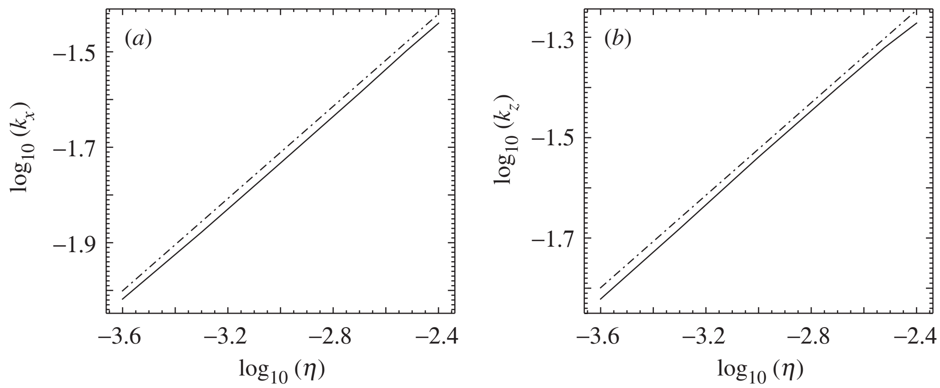

Figure 6. Relationship between k_x, k_z and η (gradient = 0.5) in both cases. The dot-dashed line is the (displaced) least-squares fit.

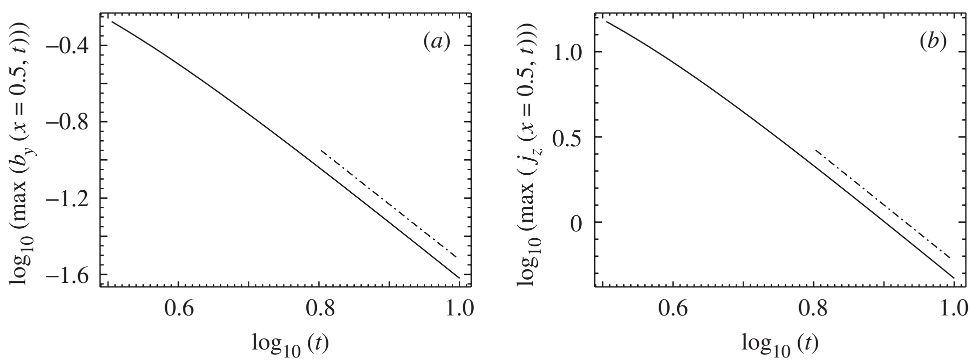

Figure 7. The decay rate for the bipolar pulse of (a) $\max(b_y)$ and (b) j_z at $x = 0.5$. The dot-dashed line is the (displaced) least-squares fit with (a) gradient $= -2.91$ and (b) gradient $= -3.32$.

$$U(x,z,t=0) = \begin{cases} 10\pi V_{\mathrm{A}}(x)\sin(10\pi(z-\frac{3}{10})), & \frac{2}{10} < z < \frac{4}{10}, \\ -10\pi V_{\mathrm{A}}(x)\sin(10\pi(z-\frac{1}{10})), & 0 < z < \frac{2}{10}, \\ 0, & \text{elsewhere.} \end{cases} \tag{4.2}$$

The two pulses can be considered to behave as the superposition of two single pulses. Each spreads out and begins to take on the Gaussian shape. However, because the pulses are of opposite sign, they cancel as they diffuse towards each other, causing a more rapid decay than before. The maximum of b_y is shown in figure 7 as a function of time, along with the maximum of the current, and the decay rate is now nearly -3. The solution is no longer fitted by a single Gaussian, but instead appears to be tending towards a shape of the form

$$b_y = A(z-z_1)\mathrm{e}^{-(z-z_1)^2/2d^2}. \tag{4.3}$$

This is shown in figure 8. The maximum of the exponential, at $z = z_1$, is propagating at the local Alfvén speed and is given by

$$z_1 = v_{\mathrm{A}}(x)t.$$

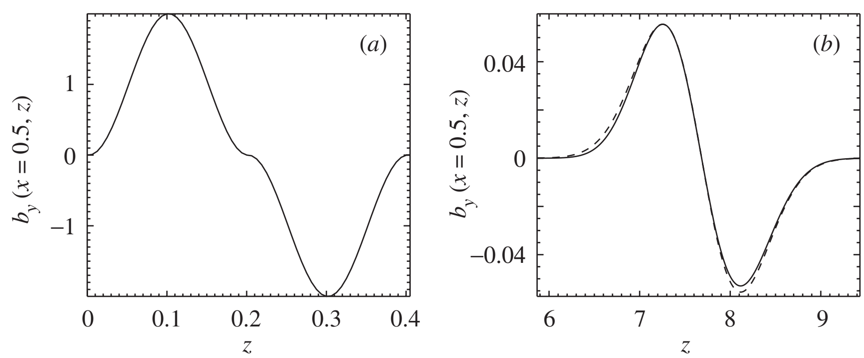

Figure 8. (*a*) The shape of the initial pulse at time $t = 0.002$. (*b*) The pulse at time $t = 7.5$. The dashed curve is the fit based on (4.3).

The widths, as given by d_x and d_z, are the same as in the single pulse, but the amplitude behaves like

$$A = k_2 t^{-3}.$$

The constant k_2 depends on the value of η and the actual Alfvén speed profile. We obtain

$$k_2 = c_2 \eta^{-1}.$$

5. Analytic theory

To obtain a simple analytical expression for the wave propagation in (2.2), we expand b_y in powers of ϵ and assume that there are two different time-scales present, namely the Alfvén wave time-scale and the slower dissipation time-scale. Thus we set

$$T_0 = t, \qquad T_1 = \epsilon t, \tag{5.1}$$

where the expansion parameter, ϵ, is related to the small dissipation coefficient η in a manner to be determined. Therefore, we set

$$b_y = b_{y0}(x, z, T_0, T_1) + \epsilon b_{y1}(x, z, T_0, T_1) + \cdots . \tag{5.2}$$

Substituting into (2.2) gives the leading-order equation as

$$\frac{\partial^2 b_{y0}}{\partial T_0^2} = V_{\mathrm{A}}^2(x) \frac{\partial^2 b_{y0}}{\partial z^2}, \tag{5.3}$$

with the solution of the form

$$b_{y0} = F(z - V_{\mathrm{A}}(x) T_0, x, T_1). \tag{5.4}$$

The function F is determined by initial conditions and a solvability condition at the next order in ϵ.

At order ϵ the equation becomes

$$\frac{\partial^2 b_{y1}}{\partial T_0^2} - V_{\mathrm{A}}^2(x) \frac{\partial^2 b_{y1}}{\partial z^2} = -2 \frac{\partial^2 b_{y0}}{\partial T_0 \partial T_1} + \frac{\eta}{\epsilon} \frac{\partial^3 b_{y0}}{\partial T_0 \partial x^2}. \tag{5.5}$$

Recall that the resistivity, η, is a small parameter and the final term of (5.5) reflects the effect of magnetic diffusion at order ϵ. The relationship between η and ϵ will be determined shortly. There will be secular terms unless the right-hand side is identically zero. Setting the right-hand side to zero, it is clear that the resulting equation for b_{y0} may be integrated in T_0, leaving a diffusion equation of the form

$$2\frac{\partial b_{y0}}{\partial T_1} = \frac{\eta}{\epsilon}\frac{\partial^2 b_{y0}}{\partial x^2}. \tag{5.6}$$

The form of solution is assumed to be

$$b_{y0} = f(T_1)F(\xi) \quad \text{and} \quad \xi = g(T_1)(z - V_{\mathrm{A}}(x)T_0), \tag{5.7}$$

where the functions f and g must be determined from (5.6). Then substituting (5.7) into (5.6) gives

$$2f'F + 2fg'(z - V_{\mathrm{A}}(x)T_0)F' = \frac{\eta}{\epsilon}(fg^2(V_{\mathrm{A}}'(x))^2T_0^2F'' - fgT_0V_{\mathrm{A}}''F'). \tag{5.8}$$

This is now rewritten in terms of the variables ξ and T_1 as

$$2f'F + 2\left(\frac{fg'}{g}\right)\xi F' = \frac{\eta}{\epsilon^3}(fg^2(V_{\mathrm{A}}'(x))^2T_1^2F'' - \epsilon fgT_1V_{\mathrm{A}}''F'). \tag{5.9}$$

The leading-order term on the right-hand side is the first term and the second term is dropped. It is clear that the correct choice for the small parameter ϵ is $\eta^{1/3}$. To solve (5.9), we select the functions f and g such that, if (5.9) is regarded as a differential equation for $F(\xi)$, the coefficients are independent of T_1. This implies two relationships must hold, namely

$$2g' = -a(V_{\mathrm{A}}'(x))^2T_1^2g^3 \tag{5.10}$$

and

$$2f' = -b(V_{\mathrm{A}}'(x))^2T_1^2fg^2, \tag{5.11}$$

where a and b are constants. The function F satisfies the equation

$$F'' + a\xi F' + bF = 0. \tag{5.12}$$

Solving (5.10) gives $g(T_1)$ as

$$g(T_1) = (\sigma^2 + \tfrac{1}{3}aV_{\mathrm{A}}'^2T_1^3)^{-1/2}, \tag{5.13}$$

where $\sigma = 1/g(0)$ is a constant connected to the initial pulse profile and

$$f(T_1) = [g(T_1)]^{b/a}. \tag{5.14}$$

Hence

$$b_{y0} = \frac{1}{[\sigma^2 + \frac{1}{3}a(V_{\mathrm{A}}')^2T_1^3]^{(b/2a)}}F\left[\frac{z - V_{\mathrm{A}}t}{(\sigma^2 + \frac{1}{3}a(V_{\mathrm{A}}')^2T_1^3)^{1/2}}\right]. \tag{5.15}$$

Now returning to (5.12), there are two distinct types of solution, depending on the value of the constant a.

(a) Harmonic case, $a = 0$

Taking $a = 0$ gives

$$F'' + bF = 0, \tag{5.16}$$

and so

$$F = \exp(\mathrm{i}k\xi), \tag{5.17}$$

with $k^2 = b$. In addition, $g(T_1)$ will be constant, so we choose

$$g(T_1) = 1, \tag{5.18}$$

and

$$f(T_1) = \exp(-\tfrac{1}{6}bV_{\mathrm{A}}'^2 T_1^3). \tag{5.19}$$

Thus we retrieve the usual phase-mixing solution derived by Heyvaerts & Priest. It is difficult to use this infinite harmonic wavetrain to analyse a single pulse. The other case provides a neater approach.

(b) Parabolic cylinder case, $a \neq 0$

If a is non-zero, we may rescale the variable ξ and take $a = 1$ without any loss of generality. Setting

$$F \propto \mathrm{e}^{-\xi^2/4} D_n(\xi)$$

and substituting into (5.12), the equation may be rewritten as a parabolic cylinder equation,

$$D_n'' + (b - \tfrac{1}{2} - \tfrac{1}{4}\xi^2) D_n = 0, \tag{5.20}$$

in terms of the parabolic cylinder functions, $D_n(\xi)$ (Abramowitz & Stegun 1970). The solutions that are zero at both plus and minus infinity require

$$b - \tfrac{1}{2} = n + \tfrac{1}{2}, \tag{5.21}$$

so that

$$b = n + 1. \tag{5.22}$$

In this case, the parabolic cylinder functions can be expressed in terms of Hermite polynomials (Abramowitz & Stegun 1970) as

$$D_n(\xi) = \mathrm{e}^{-\xi^2/4} He_n(\xi).$$

Since the Hermite polynomials form a complete set of basis functions, the most general solution for b_{y0} can be expressed as

$$b_{y0} = \sum_{n=0}^{\infty} \frac{\alpha_n}{(1 + V_{\mathrm{A}}'^2 T_1^3 / 3\sigma^2)^{(n+1)/2}} \mathrm{e}^{-\xi^2/2} He_n(\xi), \tag{5.23}$$

with $\xi = (z - V_{\mathrm{A}}t)/(\sigma^2 + \tfrac{1}{3}V_{\mathrm{A}}'^2 T_1^3)^{1/2}$. The constants α_n are determined by the initial condition.

For example, consider the initial conditions with

$$b_y(x, z, 0) = K(z). \tag{5.24}$$

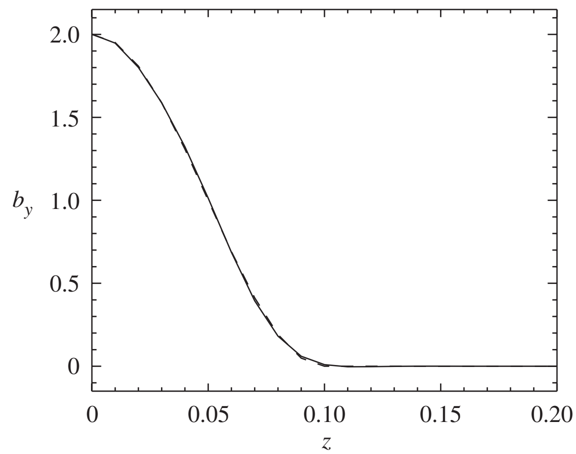

Figure 9. The initial pulse for b_y as a function of z is shown as a dashed curve and the series solution from (5.25) is the solid curve. Ten terms are used in the series and $\sigma = 0.033$.

Hence the values of α_n are given by setting

$$K(z) = \sum_{n=0}^{\infty} \alpha_n \mathrm{e}^{-z^2/2\sigma^2} He_n\left(\frac{z}{\sigma}\right). \tag{5.25}$$

Thus, using the orthogonality conditions for the Hermite polynomials, we have

$$\alpha_n = \frac{\int_{-\infty}^{\infty} K(z) He_n(z/\sigma)\,\mathrm{d}z}{\int_{-\infty}^{\infty} \mathrm{e}^{-z^2/2\sigma^2} He_n^2(z/\sigma)\,\mathrm{d}z}. \tag{5.26}$$

The denominator can be expressed as

$$\int_{-\infty}^{\infty} \mathrm{e}^{-z^2/2\sigma^2} He_n^2\left(\frac{z}{\sigma}\right) \mathrm{d}z = \sqrt{2\pi} n! \sigma. \tag{5.27}$$

However, the choice for σ still requires some thought. One possibility is to select σ to be the standard deviation of $K(z)$, but another possibility is to choose σ using a least-squares fit. The better the choice of σ, the better the convergence of the infinite series.

(*c*) *Single pulse*

Consider the numerical example used in § 3. Take

$$b_{y0}(x, z, 0, 0) = K(z) = \begin{cases} 1 + \cos(10\pi z), & |z| < 1/10, \\ 0, & \text{elsewhere}. \end{cases} \tag{5.28}$$

Since the initial profile for the individual pulse is symmetric, all the odd constants, α_{2n+1}, are zero. The shape of the initial pulse is shown in figure 9 and the approximation with ten terms is plotted for different values of σ. The least-squares fit gives $\sigma = 0.033$, which is approximately $1/10\pi$, the typical length-scale of the initial pulse. The values of α_n are given in table 1. However, it is clear from the expression for

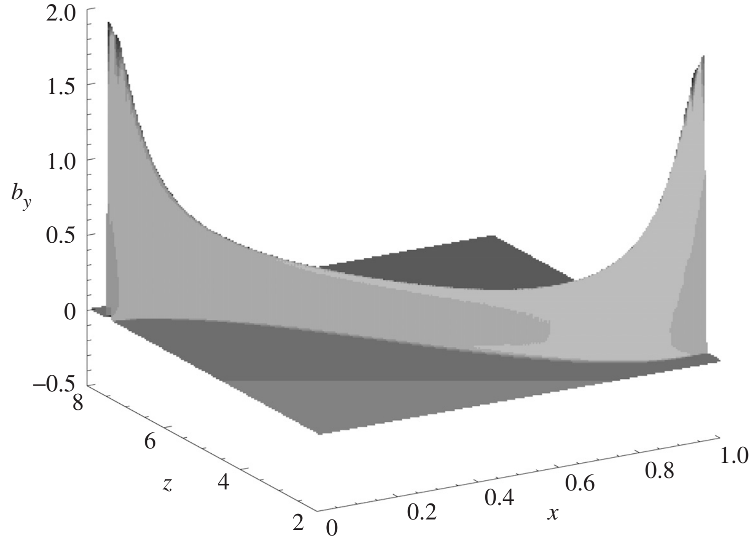

Figure 10. A surface plot of b_y at $t = 5.0$ with $\eta = 5 \times 10^{-4}$.

Table 1. *Values of* $\alpha_n \sigma^{n+1}$ *for* $\sigma = 0.033$

$\alpha_0\sigma$	$\alpha_2\sigma^3$	$\alpha_4\sigma^5$	$\alpha_6\sigma^7$
$0.1\sqrt{2/\pi}$	$1.09 \times 10^{-5}\sqrt{2/\pi}$	$-3.63 \times 10^{-9}\sqrt{2/\pi}$	$1.62 \times 10^{-13}\sqrt{2/\pi}$

$f(T_1)$ (using (5.13) and (5.14)) that the dominant term for large values of T_1 is the fundamental mode with $n = 0$. Hence, since $He_0(\xi) = 1$, the leading-order expression for b_{y0} is simply

$$b_{y0} = \frac{\alpha_0}{\sqrt{1 + V_{\mathrm{A}}'^2 \eta t^3 / 3\sigma^2}} \exp\left[\frac{-(z - V_{\mathrm{A}} t)^2}{2(\sigma^2 + \frac{1}{3} V_{\mathrm{A}}'^2 \eta t^3)}\right], \tag{5.29}$$

where

$$\alpha_0 \sigma = \frac{1}{5\sqrt{2\pi}}$$

from (5.26). This approximation, with $\sigma = 0.033$, is shown in figure 10. The maximum occurs at

$$z = V_{\mathrm{A}}(x) t.$$

For large values of t, the amplitude of b_{y0} is given by

$$\frac{1}{5\sqrt{\frac{2}{3}\pi V_{\mathrm{A}}'^2 \eta t^3}}.$$

Hence it decreases as $t^{-3/2}$, as obtained with the numerical solution. In addition, for this Alfvén speed profile, the maximum amplitude at $x = 0.5$ varies with time as

$$A = \frac{1}{5}\sqrt{\frac{6}{\pi^3}}\, \eta^{-1/2} t^{-3/2},$$

in excellent agreement with the numerical results of § 3.

The standard deviation in the vertical direction is obtained by fixing $x = 0.5$. It is given in the large-time limit by

$$d_z = \sqrt{\tfrac{1}{12}\pi^2}\eta^{1/2}t^{3/2},$$

in agreement with the numerical results. In the horizontal direction, the standard deviation is given by expanding the Alfvén speed about $x = 0.5$, so that

$$z - V_{\mathrm{A}}(x)t \approx -V_{\mathrm{A}}'(0.5)(x - 0.5)t.$$

Thus the horizontal width of the pulse increases as

$$d_x = \frac{1}{\sqrt{3}}\eta^{1/2}t^{1/2}.$$

This is again in excellent agreement with the numerical results.

Finally, the current density is approximately given by

$$j = \frac{\partial b_{y0}}{\partial x}. \tag{5.30}$$

To leading order, the large-time behaviour of j is given by

$$j = \frac{(z - V_{\mathrm{A}}(x)t)V_{\mathrm{A}}'t}{5\sqrt{2\pi}(\frac{1}{3}V_{\mathrm{A}}'^2\eta t^3)^{3/2}}\exp\left[\frac{-(z - V_{\mathrm{A}}t)^2}{\frac{2}{3}V_{\mathrm{A}}'^2\eta t^3}\right],$$

and the maximum of the amplitude of j is reached when

$$z - V_{\mathrm{A}}(x)t = [\tfrac{1}{3}(V_{\mathrm{A}}')^2\eta t^3]^{1/2}.$$

Thus the maximum of the current behaves as

$$J = \frac{3}{5}\sqrt{\frac{2}{\pi^3 \mathrm{e}}}\eta^{-1}t^{-2},$$

in agreement with the numerical results.

So an individual pulse phase mixes in a different manner to an infinite harmonic wavetrain. The damping is algebraic, rather than exponential.

(*d*) *Bipolar pulse*

Now we can use the previous theory to analyse the bipolar pulse of § 4,

$$b_{y0}(x,z,0) = K(z) = \begin{cases} 1 - \cos(10\pi z), & |z - \frac{1}{10}| < \frac{1}{10}, \\ -1 + \cos(10\pi z), & |z + \frac{1}{10}| < \frac{1}{10}, \\ 0, & \text{elsewhere.} \end{cases} \tag{5.31}$$

The pulse is now antisymmetric about $z = 0$. Hence, using (5.26), all the even constants α_{2n} will be zero this time and the pulse will remain antisymmetric. The leading-order term in the series will be the first term, so that, noting $He_1(\xi) = \xi$,

$$b_{y0} = \frac{\alpha_1}{1 + V_{\mathrm{A}}'^2\eta t^3/3\sigma^2}\frac{(z - V_{\mathrm{A}}t)}{\sqrt{\sigma^2 + \frac{1}{3}V_{\mathrm{A}}'^2\eta t^3}}\exp\left[\frac{-(z - V_{\mathrm{A}}t)^2}{2(\sigma^2 + \frac{1}{3}V_{\mathrm{A}}'^2\eta t^3)}\right], \tag{5.32}$$

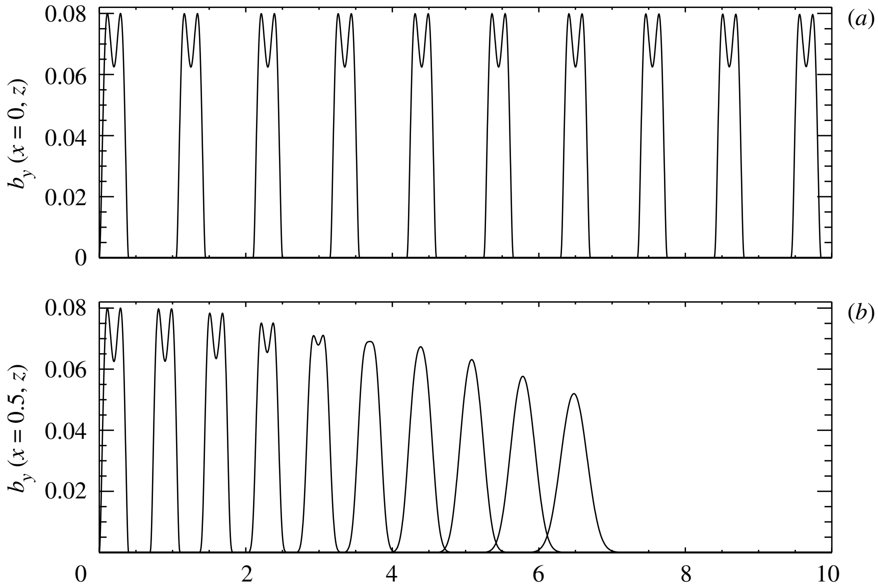

Figure 11. (a) The shape of the pulse for b_y as a function of z is shown, from left to right, at times $t = 0, 0.7, 1.4, 2.1, 2.8, 3.5, 4.2, 4.9, 5.6, 6.3$ for $x = 0.0$. (b) The shape of the pulse for b_y as a function of z is shown, from left to right, at the same times as in (a), but for $x = 0.5$.

with

$$\alpha_1 \sigma^2 = \frac{1}{50}\sqrt{\frac{2}{\pi}},$$

from (5.26). The maximum in b_{y0} occurs at

$$\xi = 1 \quad \Rightarrow \quad z - V_{\mathrm{A}} t = \sqrt{\sigma^2 + \tfrac{1}{3} V_{\mathrm{A}}'^2 \eta t^3}.$$

Thus, in the large-t limit, we have

$$\max(b_{y0}) = \frac{3}{50 V_{\mathrm{A}}'^2}\sqrt{\frac{2}{\mathrm{e}\pi}\frac{1}{\eta t^3}}.$$

This has a faster decay rate than the single pulse result and agrees with the numerical results.

6. Discussion and conclusions

A high-order finite-difference scheme has been used to investigate how individual Alfvénic pulses propagate in the inhomogeneous plasma inside a coronal hole. Since the waves are linear and there are no possibilities of shocks forming, the scheme provides an ideal way to study wave damping through resistivity.

The damping of a single pulse due to phase-mixing is substantially different from an infinite sinusoidal wavetrain. Instead of the rapid exponential damping, the dominant term now damps algebraically. Regardless of the shape of the initial pulse, it rapidly transforms into a Gaussian profile, in a manner described in § 5. The transformation of the arbitrary initial pulse into a Gaussian shape is clearly demonstrated in figure 11, where the initial pulse is obviously non-Gaussian. The peaks slowly merge together and the overall width of the pulse increases as the amplitude decreases. The Gaussian profile is perhaps not too surprising, since neglecting the advection term, $\partial^2 b_y/\partial z^2$, in (2.2) leaves the equation as the time derivative of a diffusion equation. Because the initial pulse is finite in spatial extent, we may approximate it by a delta function, point source. The standard solution to the diffusion equation is the similarity solution of the form $\exp(-x^2/\eta t)/\sqrt{t}$. However, regardless of the shape of the initial pulse and the slower algebraic decay, the typical time-scale for damping still scales with the resistivity to the power $-\frac{1}{3}$.

Two pulses of opposite sign damp faster, although still algebraically. The reason for the more rapid decay is due to the fact that as both pulses diffuse towards each other and broaden, the opposite signs cancel. The faster cancelling of the pulse gives rise to a more rapid dissipation of magnetic energy and corresponding increase in ohmic heating. An alternative way of thinking of this is to consider the single pulse. The leading and trailing edges can diffuse outwards unopposed. Thus the magnetic field gradients and, therefore, currents are reduced. When there are two pulses of opposite sign, the leading and trailing edges will still diffuse out, but the internal edges of the opposite sign diffuse into each other and, as they cancel, maintain a larger magnetic field gradient and current. Thus the ohmic dissipation is larger at the internal edges than at the external edges. The infinite wavetrain does not have the individual leading and trailing edges. Hence the dissipation will be faster in this case. Why the single pulse and the bipolar pulse should decay algebraically and the infinite wavetrain exponentially will be investigated in a subsequent paper.

The dissipation of the Alfvén pulse is calculated in terms of time but, since the pulse is propagating at the local Alfvén speed, this can be translated into a height at which the maximum ohmic heating occurs. For a single pulse given by (5.29), we have

$$b_{y0} \propto \frac{1}{\sqrt{\sigma^2 + \frac{1}{3}V_{\mathrm{A}}'^2 \eta t^3}} \exp\left[\frac{-(z - V_{\mathrm{A}} t)^2}{2(\sigma^2 + \frac{1}{3}V_{\mathrm{A}}'^2 \eta t^3)}\right], \tag{6.1}$$

and the dominant term in the current, using only $j_z = \partial b_{y0}/\partial x$, is

$$j_z \propto \frac{-(z - V_{\mathrm{A}} t) V_{\mathrm{A}}' t}{(\sigma^2 + \frac{1}{3}V_{\mathrm{A}}'^2 \eta t^3)^{3/2}} \exp\left[\frac{-(z - V_{\mathrm{A}} t)^2}{2(\sigma^2 + \frac{1}{3}V_{\mathrm{A}}'^2 \eta t^3)}\right]. \tag{6.2}$$

This is a valid approximation, since the value of j_x remains asymptotically smaller than j_z. Hence the maximum in the ohmic heating is given by the maximum of ηj_z^2, namely

$$\eta j_z^2 \propto \frac{\eta (V_{\mathrm{A}}')^2 t^2}{\left(\sigma^2 + \frac{1}{3}V_{\mathrm{A}}'^2 \eta t^3\right)^3}, \tag{6.3}$$

and the maximum of this occurs at a time

$$t = \left(\frac{6\sigma^2}{7(V_{\mathrm{A}}')^2 \eta}\right)^{1/3}. \tag{6.4}$$

Given that σ is related to the width of the initial pulse, the time to maximum damping may vary over a substantial range. In addition, this time varies inversely with the gradient of the background Alfvén speed profile.

For a coronal hole, we take $2L = 100$ Mm and $V_{A0} = 500\ \mathrm{km\,s^{-1}}$. The appropriate values for a plume would be $2L = 10$ Mm and $V_{A0} = 1000\ \mathrm{km\,s^{-1}}$. We assume a density difference of a factor of three between the low- and high-density regions within a coronal hole and of ten for a plume. The diffusivity is taken as $\eta = 1\ \mathrm{m^2\,s^{-1}}$, with a dimensionless value of approximately 10^{-11}.

The shape of the initial pulse depends on the mechanism for generating it. It has a characteristic length-scale associated with it. In our example, the dimensionless length-scale is $1/10\pi \approx \sigma$, giving the time-scale of the driver as $\tau = \sigma/V_A$. If the length-scale for the Alfvén speed profile is L, such that $V_A' \approx V_A/L$, then (6.4) gives the time for the maximum dissipation as

$$t_{\max} \approx \left(\frac{L^2\tau^2}{\eta}\right)^{1/3}. \tag{6.5}$$

The same calculation for the infinite wavetrain, using the Heyvaerts & Priest result, with the driving frequency ω giving the time-scale $\tau = 1/\omega$, suggests that $z_{\max}$ is the same as the single-pulse case but that the maximum ohmic dissipation is slightly larger.

Thus the maximum ohmic heating occurs at approximately the same height for the pulse and the infinite wavetrain, but the magnetic energy is dissipated over a larger height range for the single pulse and the maximum value is slightly lower than for the infinite wavetrain.

The pulses are assumed to remain linear throughout their existence. This assumption may need to be relaxed in subsequent work. For example, Nakariakov *et al.* (2000) have investigated how a linear wave will increase in amplitude as it propagates into a gravitationally stratified atmosphere. The increasing amplitude means that nonlinear terms must become important at some height. This effect has been ignored in the present paper. Verwichte *et al.* (1999) investigated the nonlinear evolution of an Alfvén pulse in a uniform plasma. The Alfvén pulse is taken as a Gaussian shape and it steepens to form a shock in a time given by

$$\tau_{\text{shock}} = \frac{\Delta z}{a^2 V_A},$$

where Δz is the approximate width of the Alfvén pulse, a is the dimensionless initial amplitude of the magnetic field disturbance (measured in units of the background field strength B_0) and V_A is the assumed constant background Alfvén speed. If this time is shorter than the typical dissipation time, $t_{\max}$, listed above, then nonlinearities will becomes important. For a coronal Alfvén speed of $1000\ \mathrm{km\,s^{-1}}$, the amplitude of the velocity perturbation must be less than $10\ \mathrm{km\,s^{-1}}$ in order to ignore nonlinear effects. However, it is not obvious whether the shock-formation time quoted carries over to the present case of a horizontally inhomogeneous plasma, but it is worthy of further investigation.

More detailed investigations of the propagation of wave packets must be undertaken since the recent Solar and Heliospheric Observatory observations frequently detect wave motions involving at most a couple of periods.

The numerical simulations were carried out on the JREI/SHEFC funded parallel computer. The authors thank the Particle Physics and Astronomy Research Council for financial support.

References

Abramowitz, M. & Stegun, I. 1970 *Handbook of mathematical functions.* New York: Dover.

Botha, G. J. J., Arber, T. D., Nakariakov, V. M. & Keenan, F. P. 2000 A developed stage of Alfvén wave phase mixing. *Astron. Astrophys.* **363**, 1186–1194.

Cally, P. S. 1991 Phase-mixing and surface-waves—a new interpretation. *J. Plasma Phys.* **45**, 453–479.

De Moortel, I., Hood, A. W., Ireland, J. & Arber, T. D. 1999 Phase mixing of Alfvén waves in a stratified and open atmosphere. *Astron. Astrophys.* **346**, 641–651.

De Moortel, I., Hood, A. W. & Arber, T. D. 2000 Phase mixing of Alfvén waves in a stratified and radially diverging, open atmosphere. *Astron. Astrophys.* **354**, 334–348

DeForest, C. E., Hoeksema, J. T., Gurman, J. B., Thompson, B. J., Plunkett, S. P., Howard, R., Harrison, R. & Hassler, D. M. 1997 Polar plume anatomy: results of a coordinated observation. *Solar Phys.* **175**, 393.

DeForest, C. E., Plunkett, S. P. & Andrews, M. D. 2001 Observation of polar plumes at high solar altitudes. *Astrophys. J.* **546**, 569–575.

Heyvaerts, J. & Priest, E. R. 1983 Coronal heating by phase-mixed shear Alfvén waves. *Astron. Astrophys.* **117**, 220–234.

Hood, A. W., Ireland, J. & Priest, E. R. 1997 Heating of coronal holes by phase mixing. *Astron. Astrophys.* **318**, 957–962.

Mann, I. R., Wright, A. N. & Hood, A. W. 1997 Multiple-timescales analysis of ideal poloidal Alfvén waves. *J. Geophys. Res.* **102**, 2381–2390.

Nakariakov, V. M., Ofman, L. & Arber, T. D. 2000 Nonlinear dissipative spherical Alfvén waves in solar coronal holes. *Astron. Astrophys.* **353**, 741–748.

Nocera, L., Leroy, B. & Priest, E. R. 1984 Phase mixing of propagating Alfvén waves. *Astron. Astrophys.* **133**, 387–394.

Parker, E. N. 1991 The phase mixing of Alfvén waves, coordinated modes, and coronal heating. *Astrophys. J.* **376**, 355–363.

Ruderman, M., Nakariakov, V. & Roberts, B. 1998 Alfvén wave phase mixing in two-dimensional open magnetic configurations. *Astron. Astrophys.* **338**, 1118–1124.

Sakurai, T. & Granik, A. 1984 Generation of coronal electric currents due to convective motions on the photosphere. 2. Resonance and phase mixing of Alfvén waves. *Astrophys. J.* **277**, 404–414.

Steinolfson, R. S. 1985 Resistive wave dissipation on magnetic inhomogeneities: normal-modes and phase mixing. *Astrophys. J.* **295**, 213–219.

Verwichte, E., Nakariakov, V. M. & Longbottom, A. W. 1999 On the evolution of a nonlinear Alfvén pulse. *J. Plasma Phys.* **62**, 219–232.